



Article

# Aging of Solvent-Casting PLA-Mg Hydrophobic Films: Impact on Bacterial Adhesion and Viability

Verónica Luque-Agudo <sup>1,2,3</sup>, Daniel Romero-Guzmán <sup>1,2,3</sup>, María Fernández-Grajera <sup>1,2,3</sup>, M. Luisa González-Martín <sup>1,2,3,\*</sup> and Amparo M. Gallardo-Moreno <sup>1,2,3</sup>

- Department of Applied Physics, University of Extremadura, 06006 Badajoz, Spain; vluque@unex.es (V.L.-A.); daniromero@unex.es (D.R.-G.); mariafg@unex.es (M.F.-G.); amparogm@unex.es (A.M.G.-M.)
- Networking Research Center on Bioengineering, Biomaterials and Nanomedicine (CIBER-BBN), 06006 Badajoz, Spain
- University Institute of Extremadura Sanity Research (iNube), 06006 Badajoz, Spain
- \* Correspondence: mlglez@unex.es; Tel.: +34-92426727

Received: 31 October 2019; Accepted: 29 November 2019; Published: 2 December 2019



**Abstract:** Biomaterials used for the manufacture of biomedical devices must have suitable surface properties avoiding bacterial colonization and/or proliferation. Most biomaterial-related infections start during the surgery. Bacteria can begin colonization of the surface of a device right after implantation or in the next few hours. This time may also be sufficient to begin the deterioration of a biodegradable implant. This work explores the surface changes that hydrophobic films of poly(lactic) acid reinforced with Mg particles, prepared by solving-casting, undergone after in vitro degradation at different times. Hydrophobicity, surface tension, zeta potential, topography, and elemental composition were obtained from new and aged films. The initial degradation for 4 h was combined with unspecific bacterial adhesion and viability tests to check if degraded films are more or less susceptible to be contaminated. The degradation of the films decreases their hydrophobicity and causes the appearance of a biocompatible layer, composed mainly of magnesium phosphate. The release of Mg<sup>2+</sup> is very acute at the beginning of the degradation process, and such positive charges may favor the electrostatic approach and attachment of *Staphylococci*. However, all bacteria attached on the films containing Mg particles appeared damaged, ensuring the bacteriostatic effect of these films, even after the first hours of their degradation.

Keywords: poly(lactic) acid; hydrophobicity; solvent-casting; S. epidermidis; bacterial adhesion

# 1. Introduction

Composite materials based on polymers provide an excellent platform for tailoring properties according to specific applications. Poly(lactic) acid (PLA) is one of the mostly used polymers in the market of biodegradable medical devices. The interest arises from its appropriate combination of biocompatibility and biodegradability rate. Nevertheless, some drawbacks limit its use. Poor compressive strength and the generation of acidic products during degradation limit the range of its applications [1,2]. To overcome these flaws several composites of PLA are being developed, based on copolymerization, reinforcement with carbon fibers, carbon nanotubes, hydroxyapatite (HA) or metallic particles [3–6].

Magnesium, Mg<sup>2+</sup>, is the fourth most present cation in human body. It has an essential role in the physiology of brain, heart, and skeletal muscles. It plays relevant functions in intracellular processes, as enzymatic activities, DNA repair and exchange of sodium and potassium through membranes. 99% of magnesium in body is found in bone, muscles and non-muscular soft tissue, and approximately 50%–60% of magnesium appears as surface substituent of the bone hydroxyapatite [7].

Coatings 2019, 9, 814 2 of 13

Despite the adequate biocompatibility of magnesium, its use as biomaterial is limited because its low surface stability and its fast corrosion rate in aqueous media, especially when media contain chloride. Degradation of magnesium leads to hydrogen release and increase of the pH. Moreover, fast corrosion can untimely deteriorate implants before tissue has healed. Therefore, development of biocompatible materials that slow down the production of  $Mg^{2+}$  and  $H_2$  bubbles is an interesting and important field of research [8,9].

To this purpose, new composites have been developed to improve the mechanical properties of PLA. These composites incorporate magnesium in the form of needles, wires, nanoparticles, particles [10,11], alloy fibers [12], and oxides [13,14]. Creep strength, hardness, and rigidity [15] are the main mechanical properties of PLA enhanced by these inclusions of magnesium.

In addition, the manufacturing method provides these composites with different surface properties depending on the protocol followed [1,2,10,16,17].

Surface properties, together with bulk and mechanics characteristics of the material, must be considered in detail for a successful design of an implant as far as interaction between the implant and the biological medium happens through the surface. Properties such as topography, surface electrical potential, hydrophobicity, and surface free energy can modulate the formation of a precursor layer of proteins and the subsequent adhesion and proliferation of cells [18]. Moreover, in the case of degradable materials, whose surface is continuously altered, it is necessary to follow the evolution of their surface properties with aging.

One of the most detrimental factors that can affect an implant is its colonization with bacteria, as it is the origin of infectious processes. Infection is one of the main causes, along with debridement for joint implants, leading to the removal of an implant. Half of the device-related infections are nosocomial [19], being the microbial contamination acquired along the surgical procedure. The patient's own skin, clothing and surgical instruments inside the operating room are a source of contamination. This implies that the implant can enter already contaminated in the patient or that the bacteria, through the open wound in surgery, can access the implant a few hours after placement.

Although magnesium is an essential ion for the enzymes activity and can enhance coating formation on bacterial biofilms, it has also interesting properties against bacteria contamination [20–23]. The mechanisms behind this antibacterial effect are the alkalinization of the surrounding media and the great osmotic stress originated on the cells by the ingestion of magnesium ions [22–24].

As for pure magnesium, composites materials using this metal also present these effects [25,26]. In a previous study on extruded bars of Mg with PLA, we proved that bacteria adhered on the surface of the composite were damaged [27].

In the present work we study the surface properties, degradation and bacterial response of thin films of PLA reinforced with 10% (w/w) of Mg particles prepared by solvent casting. According to Cifuentes et al. [11] this Mg proportion is a compromise solution between two factors: the generation of acidic products by the degradation of PLA, that decreases the pH, and the alkalinization due to Mg corrosion. Films of this composite were manufactured following a different procedure [28] and provided rough surfaces with water contact angle below  $90^\circ$  that could favor cell interactions. Our purpose is the analysis of films that could be used as coating for other supports to protect them against bacterial contaminations, avoiding the use of antibiotics and within a biocompatible environment. Contamination of the films with Staphylococcus epidermidis, one of the main microorganisms responsible of nosocomial infections [29] on new and aged surfaces, to simulate two possible scenarios for the contamination of the implant was investigated.

#### 2. Materials and Methods

## 2.1. Sample Preparation

The poly(lactic) acid (PLA) particles (PLA2003D, with D-isomer content of 4.25%, purchased from NatureWorks LLC, Blair, NE, USA) were dissolved in chloroform (5% w/v) using a rotator

Coatings 2019, 9, 814 3 of 13

stirrer (JP Selecta, Abrera, Barcelona, Spain). For preparation of films with magnesium (PLA10Mg), magnesium particles ( $\leq 50~\mu m$ , Nitroparis, Castellón, Spain) were added (10%~w/w) to the solved polymer and stirred until complete homogenization. 1 mL of mixture, with and without magnesium, was placed in casts of 30 mm in diameter and left at room temperature for 8 h. After that, films were dried at 70 °C in an oven for 48 h, to completely remove any remaining solvent. Disks of 25 mm diameter were cut to perform further experiments.

#### 2.2. Surface Structure Characterization

Morphology of surface of PLA films was evaluated by using an atomic force microscope (AFM) (Agilent AFM 5500, Agilent Technologies, California, CA, USA) operating at room temperature. Rectangular silicon cantilevers used have a nominal spring constant of 0.03 N m $^{-1}$  and a specified tip radius of ~8 nm (CSC38/Cr-AlBs series, MikroMash, Sofia, Bulgaria). The quantification of the surface roughness was made through the root mean square (RMS) parameter and for this purpose images of 15  $\times$  15  $\mu m^2$  were scanned. Distribution of magnesium particles in the composite was observed with a scanning electron microscope (SEM, FEI Company, Quanta 3D FEG, Hillsboro, OR, USA). The operation was done under low vacuum conditions, avoiding any metallic coating of the films. Images were taken in the backscattered electron detector (BSED) mode and energy dispersive X-Ray (EDX) mode was used to provide the elemental analysis of the films.

### 2.3. X-Ray Diffraction

XRD was performed using a Bruker D8 Advance (Rheinstetten, Germany), with Bragg–Brentano geometry and CuK  $\alpha_1$  radiation ( $\lambda = 1.5406$  Å).

#### 2.4. Surface Tension

The surface tension components of PLA and PLA10Mg films were evaluated using contact angle determinations under ambient conditions.

The measurements were carried out with a Krüss goniometer (Krüss, Hamburg, Germany) by the sessile drop method and using the Drop Shape Analyser software (Krüss GmbH, Hamburg, Germany). The values of contact angle are the average of at least nine drops deposited on different samples and reported with the standard deviation.

In the experiment, three liquids were used: deionized water, formamide, and diiodomethane, whose surface tension components are well-known [30].

The surface tension components of the films were calculated with Equation (1) using the approach of van Oss et al. [31–33].

$$(1 + \cos \theta)\gamma_i^{TOT} = 2\left(\sqrt{\gamma_i^{LW}\gamma_s^{LW}} + \sqrt{\gamma_i^-\gamma_s^+} + \sqrt{\gamma_i^+\gamma_s^-}\right),\tag{1}$$

where  $\theta$  is the contact angle between the liquid and the surface,  $\gamma^{LW}$  is the Lifshitz–van der Waals surface tension component,  $\gamma^+$  represents the electron acceptor parameter,  $\gamma^-$  represents the electron donor parameter,  $\gamma^{TOT} = \gamma^{AB} + \gamma^{LW}$  is the total surface tension component and  $\gamma^{AB}$  is the Lewis acid-base component, with  $\gamma^{AB} = 2\sqrt{\gamma^+\gamma^-}$ . The subindex i represents the surface tension component of the liquids and subindex s the surface tension component of the surface.

The degree of hydrophobicity of a material can be estimated as the free energy of interaction between two surfaces of the same material immersed in water:  $\Delta G_{sws}$  (Equation (2)) [34]. In this approach, if  $\Delta G_{sws} < 0 \text{ mJ/m}^2$ , the material is considered hydrophobic and if  $\Delta G_{sws} > 0 \text{ mJ/m}^2$ , the material is considered hydrophilic.

$$\Delta G_{sws} = -2 \left( \sqrt{\gamma_s^{LW}} - \sqrt{\gamma_w^{LW}} \right)^2 + 4 \left( \sqrt{\gamma_s^+ \gamma_w^-} + \sqrt{\gamma_s^- \gamma_w^+} - \sqrt{\gamma_s^+ \gamma_s^-} - \sqrt{\gamma_w^+ \gamma_w^-} \right)$$
 (2)

Coatings 2019, 9, 814 4 of 13

#### 2.5. Surface Charge

The surface charge was analysed through streaming potential and streaming current measurements by an electrokinetic analyzer (EKA) (Anton Paar, Austria). The experiments were carried out with a symmetrical cell using two identical films (25 mm of diameter). The zeta potential was calculated using the Helmholtz–Smoluchowsky equation:

$$\zeta = \frac{\eta}{\varepsilon_0 \varepsilon_r} \frac{L}{Q} \frac{dI_{str}}{dp} = \frac{\eta}{\varepsilon_0 \varepsilon_r} K \frac{dV_{str}}{dp}$$
(3)

where  $I_{str}$  and  $V_{str}$  were the streaming current and streaming potential; p is the channel pressure;  $\eta$  and  $\varepsilon_r$  are the dynamic viscosity and the permittivity of the fluid, respectively;  $\varepsilon_0$  is the permittivity of vacuum; K is the conductivity of the channel; and L and Q are the length and cross-section of the channel. All measurements were made with the same compression conditions inside the electrokinetic channel and the geometrical factor L/Q was obtained as previously described [35]. Each streaming current or potential measurement involved four cycles, two in each flow direction. The pressure was applied in a ramp form, from 0 to 600 mbar. KCl 1 mM was used as the electrolyte solution with pH 5.6.

#### 2.6. In Vitro Degradation Evaluation

Degradation of PLA and PLA10Mg films was evaluated by immersion (by triplicate) of samples of 25 mm of diameter in 50 mL of phosphate buffer saline (PBS) at 37 °C for 4 and 8 h and 1, 7, 14, 21 and 28 days. The pH of the starting PBS solution was 6.67, and after four weeks, pH increased to 6.91. After degradation, films were dried with nitrogen and stored for at least 24 h in a desiccator. Changes in the morphology of surfaces were analyzed again by AFM and SEM. Inductively coupled plasma-mass spectroscopy (ICP-MS, 7900 Agilent Technologies, California, CA, USA) was used to quantify the amount of Mg released to the PBS.

To simulate the degradation conditions in which bacterial adhesion was performed, PLA and PLA10Mg films were exposed (by triplicate) to 0.9 mL of PBS at 37 °C for 4 h with the help of reusable silicone adhesion cambers (flexiPERM, Greiner bio-one, Frickenhausen, Germany). Then, films were dried with nitrogen and stored for at least 24 h in a desiccator. AFM and SEM were used to assess the changes in topography and ICP-MS was used to determine the magnesium concentration.

# 2.7. Bacterial Adhesion Assays

Staphylococcus epidermidis ATCC 35983 (ATCC, American Type Collection Culture) was obtained. The strain was stored at -80 °C in porous beads (Microbank, ProLab Diagnostics, Richmond Hill, Ontario, Canada). From the frozen stock, blood agar plates (OXOID Ltd., Basingstoke, Hampshire, UK) were inoculated and incubated at 37 °C for 24 h to obtain cultures. The strain was then grown in trypticase soy broth (TSB) (BBL, Becton Dickinson and Company, Sparks, Franklin Lakes, New Jersey, USA) for different bacterial assays. For adhesion studies, bacteria were grown in TSB and resuspended in PBS to a final concentration of 3·10<sup>8</sup> bacteria/mL, then a volume of 0.9 mL was added to the PLA and PLA10Mg films with the help of reusable silicone adhesion chambers, previously described, and subjected to slight orbital shaking of 20 rpm, for 4 h at 37 °C. Quantification of the density of the bacteria was carried out with an epifluorescence microscope (Leitz DIAPLAN, Wetzlar, Germany) by staining the adhered microorganisms with the kit Live/Dead Baclight L-7012 (Invitrogen SA, Eugene, Oregon, USA). Bacteria were counted with the software NIS-Elements BR 4.10 (Nikon Instruments Inc., Melville, USA). These experiments provided the total number of bacteria adhered to the surface of the samples, and the viability of the cells. Bacteria appearing as red-orange have their viability compromised, whereas green bacteria are not damaged. Images were acquired from random surface positions for each sample.

The experiments were carried out in triplicate and repeated at least three times with independent cultures in order to confirm reproducibility.

Coatings 2019, 9, 814 5 of 13

#### 2.8. Statistical Analyses

For adhesion assays, the data were reported as mean values  $\pm$  S.D. from at least three independent experiments. The differences between groups were evaluated by Wilcoxon test. All statistical analyses were performed using the free software R, version 3.5.0. Differences were considered statistically significant at p-values  $\leq$  0.05.

#### 3. Results and Discussion

## 3.1. Surface of Films Characterization

BSED images of the surface and of a transversal section of a PLA10Mg film are presented in Figure 1. Transversal section of films had a thickness comprised between 40 and 50  $\mu$ m. Magnesium particles were well dispersed, without presence of aggregates or clusters. Some particles protruded from the film plane, but they stayed wrapped with a thin polymer layer. AFM images (Figure 2) confirmed the morphology of films. Profiles taken from images of PLA10Mg (Figure 2a) and PLA (Figure 2b) films gave roughness values of  $45 \pm 15$  nm and  $12 \pm 5$  nm, respectively. However, the larger RMS of PLA10Mg films was mainly related to the contribution of bumps due to particles. PLA film profile showed features no higher than 0.16  $\mu$ m. PLA10Mg profile had larger features due to magnesium protuberances, particularly, in the case of the image, they could reach to ca. 0.64  $\mu$ m height, but the surface topography between the Mg bumps was like that of the PLA film.

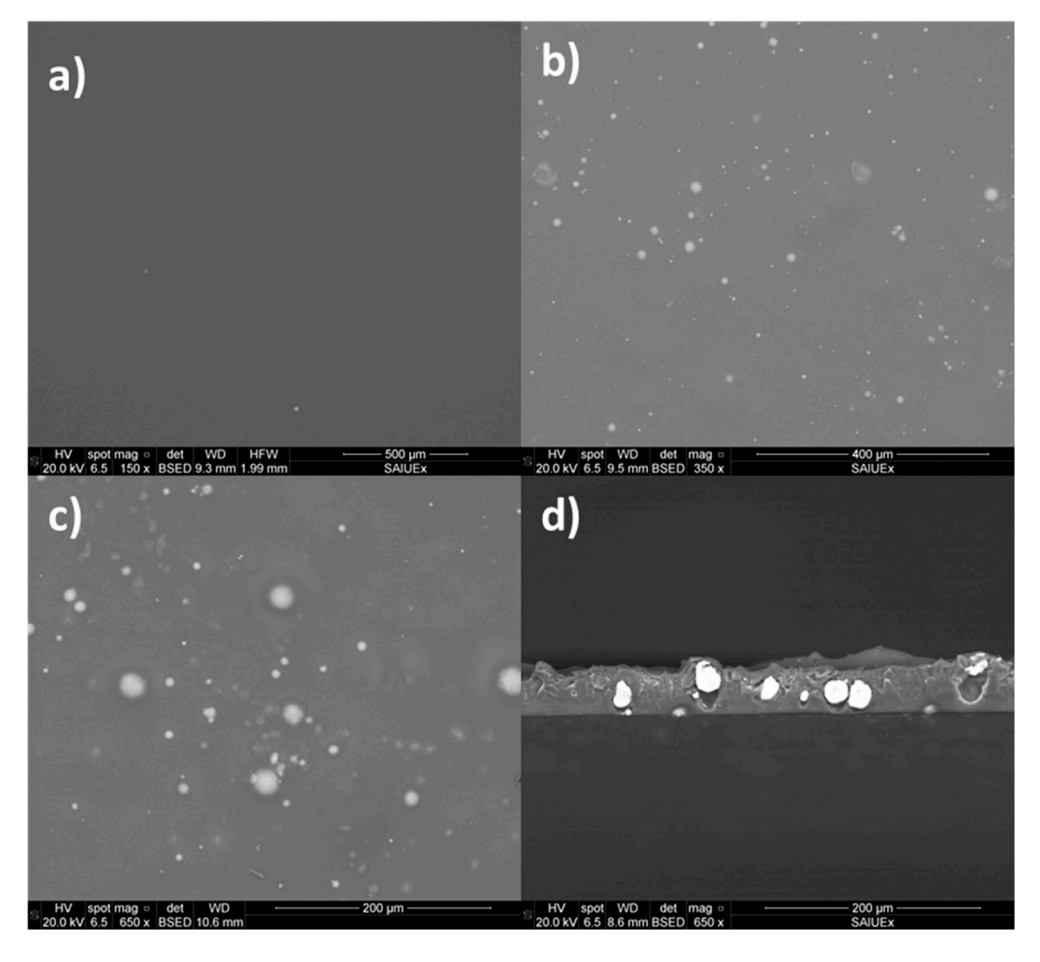


**Figure 1.** Backscattered electron detector (BSED) images from SEM of the surface of a poly(lactic) acid (PLA) film (**a**), a PLA10Mg film (**b**,**c**) and a cross-section of a PLA10Mg film (**d**). Scale bars are included at the bottom of the images. Different colours indicate different atomic numbers. In this case, white spots are related to Mg particles and grey background is related to polymer.

Coatings 2019, 9, 814 6 of 13

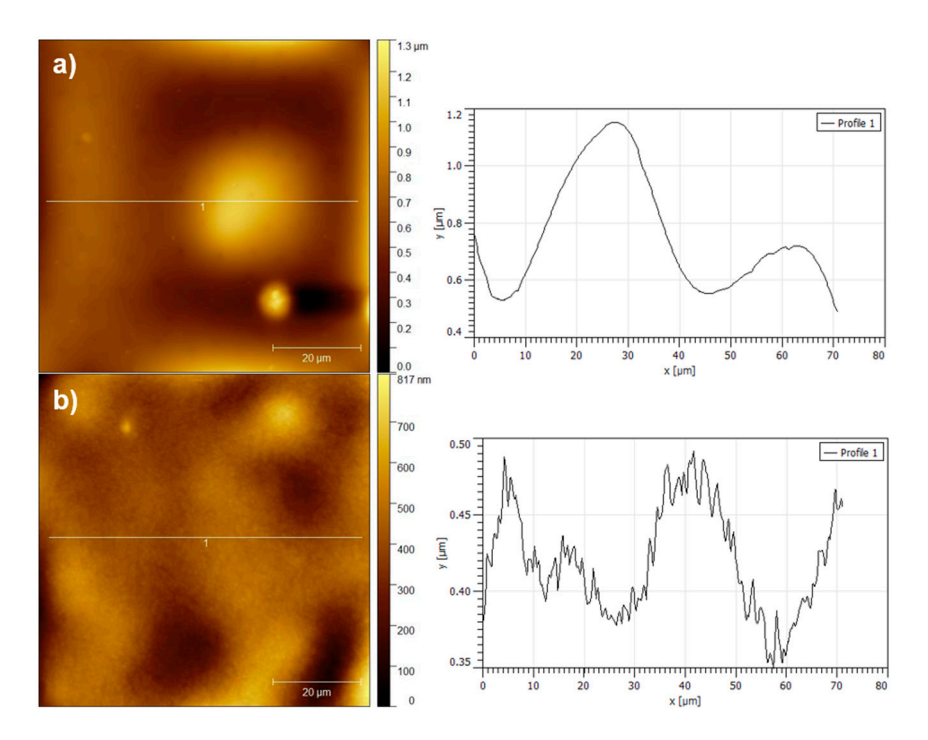


**Figure 2.** Atomic force microscope (AFM) topographical images and a representative profile (white line in topographical images) of (a) PLA10Mg film and (b) and PLA film. As it can be seen from the scale, different colors represent different heights: dark colors indicate hollows and lighter colors indicate higher areas.

The crystallinity of PLA10Mg and PLA films was evaluated by XRD (Figure 3). Diffractograms presented well defined peaks, indicating that microcrystallinity was present in both types of films. PLA film showed a pair of peaks at  $16.6^{\circ}$  and  $19.0^{\circ}$ . PLA10Mg peaks were slightly displaced to  $16.9^{\circ}$  and  $19.2^{\circ}$ .

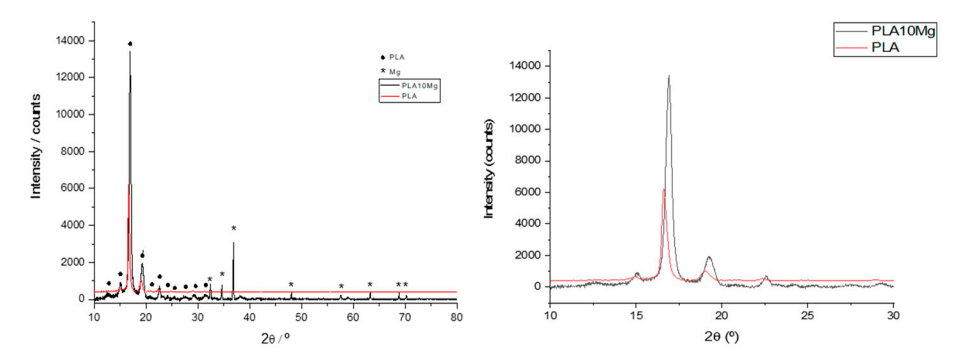


**Figure 3.** X-Ray diffractrogram of PLA10Mg and PLA films. Peaks have been assigned for the polymer and for the Mg particles. PLA10Mg (black line) and PLA (red line) presents peaks at  $14.4^{\circ}$  and  $22.5^{\circ}$ , characteristics of  $\alpha$  crystalline phase.

Both films had peaks at  $14.4^{\circ}$  and  $22.5^{\circ}$ , characteristics of  $\alpha$  crystalline phase, thus discarding the  $\delta$  phase. The small displacements of peaks may be due to some distortion in the polymer chain, but within the same crystalline phase, caused by the presence of Mg particles. This affects the packaging and spacing between chains and, therefore, the distance between reflection planes.

Contact angle of water,  $\theta_w$ , formamide,  $\theta_F$ , and diiodomethane,  $\theta_D$ , on PLA10Mg and PLA films are listed in Table 1. Within the experimental uncertainty, water and formamide contact angle were identical for both materials. Differences in roughness of both films were not reflected in the value of

Coatings 2019, 9, 814 7 of 13

the contact angle of sessile drops. Water contact angle obtained was higher than referred by other authors [36,37].

**Table 1.** Contact angles ( $\theta$ w: water,  $\theta_F$ : formamide,  $\theta_D$ : diiodomethane) of PLA10Mg and PLA new and aged films and surface free energy ( $\gamma^T$ ), components ( $\gamma^{LW}$ : Lifshitz–van der Waals,  $\gamma^{AB}$ : acid–base) and surface free energy of interaction of surfaces immersed in water ( $\Delta G_{SWS}$ ).

Sample		θ <sub>W</sub> [°]	θ <sub>F</sub> [°]	θ <sub>D</sub> [°]	$\gamma^{T}$ (mJ·m <sup>-2</sup> )	$\gamma^{LW}$ (mJ·m <sup>-2</sup> )	$\gamma^{AB}$ (mJ·m <sup>-2</sup> )	$\Delta G_{SWS}$ (mJ·m <sup>-2</sup> )
New film	PLA10Mg	106 ± 1	88 ± 1	$58 \pm 3$	$30 \pm 3$	28 ± 2	$1.9 \pm 0.6$	$-67 \pm 5$
	PLA	106 ± 2	90 ± 4	66 ± 2	25 ± 2	24 ± 1	$1.2 \pm 1.0$	$-70 \pm 10$
Aged film	PLA10Mg	97 ± 4	86 ± 4	$63 \pm 7$	$28 \pm 4$	$25 \pm 3$	$2.9 \pm 2.5$	$-48 \pm 14$
	PLA	98 ± 4	89 ± 4	64 ± 2	27 ± 3	24 ± 2	$3.4 \pm 2.3$	$-46 \pm 15$

Onder et al. [38] reported contact angles of 109.1° in PLA films prepared under a relative humidity of 33%, conditions in which the PLA surface is microporous. Authors point out that the presence of air pockets in these pores is the reason why the surface becomes hydrophobic, in agreement with conditions for superhydrophobic surfaces. The analysis of the SEM images shows that these micropores had not been formed on the surface of our PLA films and, therefore, the air pockets could not be the cause of the high hydrophobicity. On the other hand, Li et al. [39] indicated that the hydrophobicity of PLA increased when its crystallinity did, due to the orientation of the methyl groups on its surface. Thus, these authors presented for PLA a  $\theta_{\rm W}$  of 78.1° and 107.5° before and after orienting these groups, respectively. After orientation, the crystallinity of the PLA samples increased significantly, leading to a higher content of methyl groups on the surface and, therefore, to an increase of hydrophobicity. Nevertheless, surface orientation depended on the process of fabrication and thickness of the layer, among other factors [40,41], which suggests that the experimental process is decisive for modulating the final behavior of the surface hydrophobicity. In the same line, manufacturing method could also affect the arrangement and conformation of the polymer chains, within the same crystalline phase, and therefore determines the orientation of the functional groups most exposed to the surface, thus influencing hydrophobicity.

It appears that the contact angle of the apolar liquid diiodomethane was slightly lower on the PLA10Mg than on the PLA film. The higher interaction of the non-polar liquid with PLA10Mg than with PLA may be related with the slightly distortion in the crystalline phase of films, where a change in the ordination of polymer can slightly increase the number of non-polar methyl groups exposed in the surface. Nevertheless, this redistribution did not seem to be important enough to alter the interaction with water and formamide so much that  $\theta_{\text{W}}$  and  $\theta_{\text{F}}$  were modified. Table 1 includes the total surface free energy ( $\gamma^{T}$ ) and its Lifshitz–van der Waals ( $\gamma^{LW}$ ) and acid–base ( $\gamma^{AB}$ ) components for both films. According to the differences in  $\theta_D$ ,  $\gamma^{LW}$  of PLA10Mg film seemed larger than for PLA, and, since there were no differences in polar interactions, total surface energy was slightly higher for the composite film. The interaction free energy of two equal surfaces immersed in water,  $\Delta G_{SWS}$ , provides a measure of the interplay of material and water, and an accurate quantification of the hydrophobicity of the material [42]. A more negative value of  $\Delta G_{SWS}$ , indicated that interaction between the surfaces of the material or the ordination in water was favored over the interaction of surfaces with water. PLA10Mg and PLA films presented the same  $\Delta G_{SWS}$  (Table 1), within the experimental uncertainty, which confirms the same hydrophobicity for both films. However, it cannot be discarded that some magnesium ions were displaced out of the surface, being the highly hydrated Mg<sup>2+</sup> ions favoring water-water ordering.

Zeta potential ( $\zeta$ ) provides information of the surface electrical property of the samples. Using the Helmholtz–Smoluchowski approach, the values were  $-26.0 \pm 0.6$  mV for PLA10Mg and  $-35 \pm 3$  mV for PLA. The absolute value for the PLA film was slightly lower to the obtained by Kolska et al. [43]. They measured  $\zeta$  for different polymers after and before various surface treatments and pH. In the

Coatings 2019, 9, 814 8 of 13

case of pristine PLA the value was -47.5 mV at pH 7. However, Bastekova et al. [44] got for their films, whose contact angle was  $74.5^{\circ} \pm 5.8^{\circ}$ , a  $\zeta$  value of  $-67.2 \pm 5.0$  mV, measured at pH 6.5, that indicates an important negatively-charged surface. Differences in zeta potential have to be associated with the different preparation methods. On the other hand, the less negative zeta potential of PLA10Mg can be related with the release of Mg<sup>2+</sup> cations to the surrounding media during the measuring process with the EKA. Positive ions can be retained within the double layer of the material, decreasing its measured zeta potential.

We have followed the release of magnesium ions from PLA10Mg films for a period of 28 days (Figure 4). Within the first 4 h of surface immersion in PBS, the  $Mg^{2+}$  liberation is very fast and afterwards the ions release per unit area of the film progresses linearly with time (release rate equal to  $0.080~\mu g/(mm^2 \cdot day)$  or  $0.003~\mu g/(mm^2 \cdot h)$ ). The liberation of magnesium ions to the PBS media, rich in phosphate salts, allows the formation of the very insoluble magnesium phosphate. Images of transversal sections of films after 7 (Figure 5a), 14 (Figure 5b) and 21 (Figure 5c) days allowed us to visualize the progressive formation of the deposited layer on the PLA10Mg films. Figure 5d displays the extension of the deposit on the PLA10Mg film surface after 28 days of immersion. EDX analysis confirms that this layer was formed mainly by magnesium phosphate (Figure 5d, inset).

Zhang and Ma reported [45] that PLA was able to form apatite once incubated in simulated body fluid (SBF) because of the carboxylic acid groups generated during hydrolysis. This process charged the surface negatively, and thus promoted the binding to Ca<sup>2+</sup> via electrostatic forces and hydrogen bonding. Previously, it had been reported that by soaking the material in SBF, a calcium phosphate layer was formed [46,47]. The appearance of a white precipitate was already observed by Li et al. [16] when immersing PLA samples in PBS in a dynamic system, applying a load frequency of 2.5 Hz. In their case, the layer was composed of calcium and phosphor, while in ours the alkaline-earth metal is magnesium. From the study of Li et al. it can be concluded that the salt precipitates if the PLA is submerged in PBS in both static and dynamic methods, due to the poor solubility of phosphates in aqueous medium.

Amorphous magnesium phosphate (AMP) has suitable properties such as biocompatibility, biodegradability, and bioactivity [48–51]. Also, it can provide efficient protection against Mg and polymer degradation. Water contact angle measured on the PLA10Mg films aged for 28 days in PBS was  $71^{\circ} \pm 20^{\circ}$ . The large experimental uncertainty for this angle is due to the irregularities of the surface layer, as far as the deposit does not cover uniformly the film. Despite uncertainty, it appears that the presence of this deposit on the PLA10Mg film reduces its hydrophobicity.

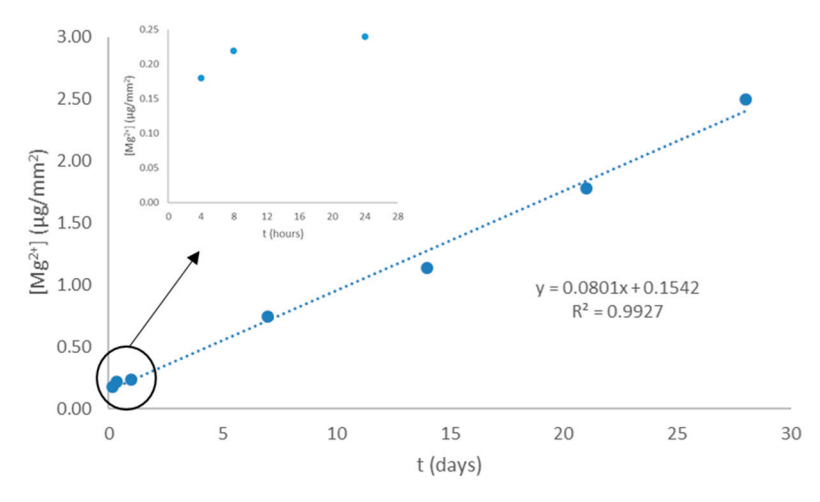
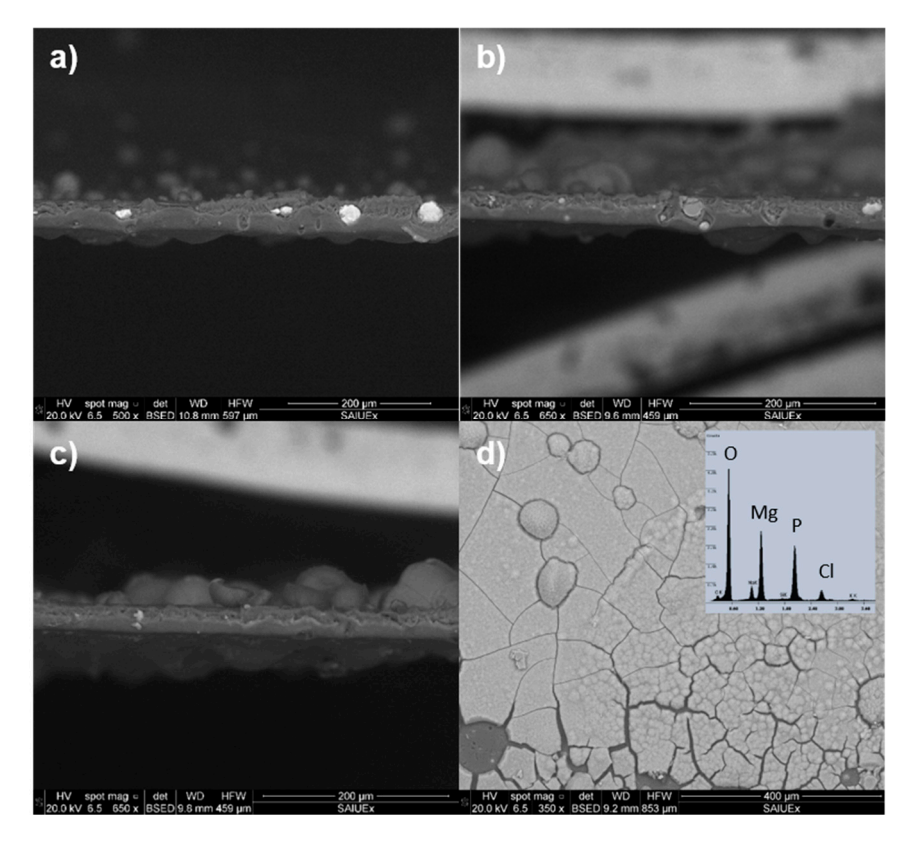


Figure 4. Mg<sup>2+</sup> release from PLA10Mg films immersed in phosphate buffer saline (PBS) over time.

Coatings 2019, 9, 814 9 of 13



**Figure 5.** SEM images of PLA10Mg films after (a) 7, (b) 14, (c) 21 and (d) 28 days of degradation. (a–c) are cross-section images, and (d) is a surface image. In (d), the EDX spectrum of the surface is included, confirming that the layer is composed of magnesium phosphate.

#### 3.2. Bacterial Adhesion

Infection is one of the main detrimental processes that can compromise implanted devices. In most cases, the bacterial contamination of the devices occurs right at the time of surgery. It takes a few hours for bacteria to bind to the surface and grow to form a biofilm. Consequently, any degradable material or coverage is intended to resist bacterial colonization when degradation has not yet started or after a short period of time after it begins. To simulate such situations two different experiments of bacterial adhesion were designed. These experiments consisted in the contact for 4 h of a suspension of S. epidermidis with PLA10Mg film and PLA film. In one case these films were new and in the other case the films were previously aged by immersion in PBS at 37 °C for 4 h. The density of adhered bacteria and viability in both experiments are shown in Table 2. The adhesion of S. epidermidis on new films of PLA10Mg was slightly lower than on new PLA films (*p*-value < 0.05, according to Wilcoxon test), but the opposite tendency happened on aged films (p-value < 0.05, according to Wilcoxon test). In relation to viability, there were huge changes when comparing the films without and with Mg particles: in both cases, new and aged films, it is remarkable that all bacteria adhered on the PLA10Mg surface appeared damaged after the adhesion experiment (p-value < 0.05 in both comparisons: new films and aged films, according to Wilcoxon test). Magnesium-based materials are bacteriostatic. Mechanisms behind this characteristic are related to the joint action of magnesium ions and the modification of the pH of the surrounding media, especially in a local range near the surface. The pH and the concentration of Mg<sup>2+</sup> ions that could have some impact on bacterial adhesion have been measured. New and aged films of PLA10Mg were immersed in PBS (pH 6.64) for 4 h, the same time as the bacterial adhesion experiments lasted. After that time, the pH and concentration of Mg<sup>2+</sup> ions were measured. The results for both experiments listed in Table 2 are similar. This is due to the low solubility of magnesium phosphates in aqueous media, leading to their saturation. The pH increase was only 0.13 units, despite the high

Coatings 2019, 9, 814 10 of 13

density of  $Mg^{2+}$  ions in the medium. It is in accordance with the important role that the polymeric matrix plays controlling the corrosion of Mg particles, hindering the alkalinization of the media.

<b>Table 2.</b> Number of adhered bacteria to surfaces, viability of adhered bacteria, Mg <sup>2+</sup> concentration and
pH of PLA10Mg new and aged films.

		Adhesion of S.  Epidermidis (Bacteria·10 <sup>4</sup> per cm <sup>2</sup> )	Viability (%)	[Mg <sup>2+</sup> ] (ppm)	рН
Ni. Pil.	PLA10Mg	110 ± 2	0	$14.33 \pm 0.92$	$6.77 \pm 0.02$
New Film	PLA	129 ± 1	100	-	$6.61 \pm 0.01$
Aged Film	PLA10Mg	138 ± 2	0	$14.79 \pm 0.54$	$6.77 \pm 0.01$
Ageu riim	PLA	120 ± 5	100	-	$6.60 \pm 0.01$

Immersion of PLA and PLA10Mg films in PBS for 4 h was sufficient to initiate the surface degradation. The RMS obtained from AFM images on PLA degraded samples increased to almost three times in relation to non-aged samples (32  $\pm$  9  $\mu$ m versus 12  $\pm$  5  $\mu$ m). However, this roughness change is not enough to affect the contact angle measurements. There are not differences between contact angles on PLA10Mg and PLA aged surfaces (Table 1). Water contact angle slightly decreases respect to the new surfaces, but no changes are obtained in formamide or diiodomethane with respect to the new PLA film. Nevertheless, it can be expected that the cations released during the ageing process, highly hydrated, retained within the Helmholtz plane will remain deposited on the surfaces when films are removed from PBS for contact angle measurements. In addition, the deposition of some precipitates on the film surface begins once degradation starts, decreasing also the hydrophobicity of the surface and the contact angle of water. Some authors have stated that hydrophobicity of the material surface plays an important role in bacterial adhesion, more than bacterial surface hydrophobicity [52]. In our case, this is difficult to confirm since similar changes in hydrophobicity, as the values of  $\Delta G_{SWS}$ in Table 1 show, in PLA and PLA10Mg before and after 4h degradation give opposite changes in bacterial adhesion: on PLA10Mg increases and on PLA decreases. As has already been suggested, the Mg<sup>2+</sup> cations released and trapped at the PLA10Mg films interface after degradation would favor the electrostatic approach and further attachment of the negative charged bacterial cells [53], increasing the number of the bacterial adhesion in 25% (Table 2). These results reinforce the idea that bacterial adhesion is the result of the joint action of different factors where it is difficult to ponder the impact of hydrophobic or electrical forces.

## 4. Conclusions

Thin films of a composite of PLA with a proportion of 10% (w/v) of magnesium particles, manufactured by solvent casting, exhibited high hydrophobicity and intense bacteriostatic behavior. The degradation of the films allowed the appearance of a biocompatible layer, composed mainly by magnesium phosphates, decreasing the hydrophobicity of the film. The release of Mg cations was carried out at a constant rate throughout the period studied, except within the first hours of degradation, when the release was very acute.

Since bacteria may begin colonization of the implants surface during the surgery or after a few hours, when a biodegradable material would have already begun to deteriorate, bacterial tests on few hours aged films provide relevant information about the material performance. *S. epidermidis* adhesion on PLA10Mg aged films increases respect to the new ones probably due to the favorable electrostatic interaction between the negatively charged cells and the more positively charged surface, because of released Mg<sup>2+</sup> ions, despite the lower hydrophobicity of degraded films. Nevertheless, the strong initial release of Mg ions from PLA10Mg films ensures that the bacteriostatic effect observed on new prepared films also takes place on aged surfaces for the first hours.

Coatings 2019, 9, 814 11 of 13

**Author Contributions:** Conceptualization, V.L.-A., M.L.G.-M., and A.M.G.-M.; formal analysis, V.L.-A., D.R.-G., M.F.-G., M.L.G.-M., and A.M.G.-M.; investigation, V.L.-A., D.R.-G., and M.F.-G.; methodology, M.L.G.-M. and A.M.G.-M.; supervision, M.L.G.-M. and A.M.G.-M.; writing—original draft, V.L.-A. and D.R.-G.; writing—review and editing, M.L.G.-M. and A.M.G.-M.

**Funding:** This research was funded by Junta de Extremadura and FEDER, grant numbers GR15089 and GR18153, and project number IB16117, and by Ministerio de Economía y Competitividad del Gobierno de España, project numbers MAT2015-63974-C4-3-R, PCIN-2016-146 and RTI2018-096862-B-I00.

Conflicts of Interest: The authors declare no conflict of interest.

#### References

- 1. Wan, P.; Yuan, C.; Tan, L.L.; Li, Q.; Yang, K. Fabrication and evaluation of bioresorbable PLLA/magnesium and PLLA/magnesium fluoride hybrid composites for orthopedic implants. *Compos. Sci. Technol.* **2014**, *98*, 36–43. [CrossRef]
- 2. Swaroop, C.; Shukla, M. Nano-magnesium oxide reinforced polylactic acid biofilms for food packaging applications. *Int. J. Biol. Macromol.* **2018**, *113*, 729–736. [CrossRef] [PubMed]
- 3. Shen, L.; Yang, H.; Ying, J.; Qiao, F.; Peng, M. Preparation and mechanical properties of carbon fiber reinforced hydroxyapatite/polylactide biocomposites. *J. Mater. Sci. Mater. Med.* **2009**, 20, 2259–2265. [CrossRef] [PubMed]
- 4. Zhang, D.; Kandadai, M.A.; Cech, J.; Roth, S.; Curran, S.A. Poly(L-lactide) (PLLA)/Multiwalled Carbon Nanotube (MWCNT) Composite: Characterization and Biocompatibility Evaluation. *J. Phys. Chem. B* **2006**, 110, 12910–12915. [CrossRef] [PubMed]
- 5. Hamada, Y.; Fujitani, W.; Kawaguchi, N.; Daito, K.; Niido, T.; Uchinaka, A.; Mori, S.; Kojima, Y.; Manabe, M.; Nishida, K.; et al. The preparation of PLLA/calcium phosphate hybrid composite and its evaluation of biocompatibility. *Dent. Mater. J.* **2012**, *31*, 1087–1096. [CrossRef] [PubMed]
- 6. Murariu, M.; Dubois, P. PLA composites: From production to properties. *Adv. Drug Deliv. Rev.* **2016**, 107, 17–46. [CrossRef]
- 7. De Baaij, J.H.F.; Hoenderop, J.G.J.; Bindels, R.J.M. Magnesium in man: Implications for health and disease. *Physiol. Rev.* **2015**, *95*, 1–46. [CrossRef]
- 8. Felfel, R.M.; Hossain, K.M.Z.; Parsons, A.J.; Rudd, C.D.; Ahmed, I. Accelerated in vitro degradation properties of polylactic acid/phosphate glass fibre composites. *J. Mater. Sci.* **2015**, *50*, 3942–3955. [CrossRef]
- 9. Abdal-Hay, A.; Dewidar, M.; Lim, J.; Lim, J.K. Enhanced biocorrosion resistance of surface modified magnesium alloys using inorganic/organic composite layer for biomedical applications. *Ceram. Int.* **2014**, 40, 2237–2247. [CrossRef]
- 10. Cifuentes, S.C.; Gavilán, R.; Lieblich, M.; Benavente, R.; González-Carrasco, J.L. In vitro degradation of biodegradable polylactic acid/magnesium composites: Relevance of Mg particle shape. *Acta Biomater.* **2016**, 32, 348–357. [CrossRef]
- 11. Cifuentes, S.C.; Frutos, E.; González-Carrasco, J.L.; Muñoz, M.; Multigner, M.; Chao, J.; Benavente, R.; Lieblich, M. Novel PLLA/magnesium composite for orthopedic applications: A proof of concept. *Mater. Lett.* **2012**, *74*, 239–242. [CrossRef]
- 12. Wu, Y.H.; Li, N.; Cheng, Y.; Zheng, Y.F.; Han, Y. In vitro Study on Biodegradable AZ31 Magnesium Alloy Fibers Reinforced PLGA Composite. *J. Mater. Sci. Technol.* **2013**, 29, 545–550. [CrossRef]
- 13. Sawai, J.; Kojima, H.; Igarashi, H.; Hashimoto, A.; Shoji, S.; Sawaki, T.; Hakoda, A.; Kawada, E.; Kokugan, T.; Shimizu, M. Antibacterial characteristics of magnesium oxide powder. *World J. Microbiol. Biotechnol.* **2000**, *16*, 187–194. [CrossRef]
- 14. Coelho, C.C.; Araújo, R.; Quadros, P.A.; Sousa, S.R.; Monteiro, F.J. Antibacterial bone substitute of hydroxyapatite and magnesium oxide to prevent dental and orthopaedic infections. *Mater. Sci. Eng. C* **2019**, 97, 529–538. [CrossRef] [PubMed]
- 15. Li, X.; Chu, C.; Zhou, L.; Bai, J.; Guo, C.; Xue, F.; Lin, P.; Chu, P.K. Fully degradable PLA-based composite reinforced with 2D-braided Mg wires for orthopedic implants. *Compos. Sci. Technol.* **2017**, *142*, 180–188. [CrossRef]
- 16. Zhao, C.; Wu, H.; Ni, J.; Zhang, S.; Zhang, X. Development of PLA/Mg composite for orthopedic implant: Tunable degradation and enhanced mineralization. *Compos. Sci. Technol.* **2017**, *147*, 8–15. [CrossRef]

Coatings 2019, 9, 814 12 of 13

17. Li, X.; Guo, C.; Liu, X.; Liu, L.; Bai, J.; Xue, F.; Lin, P.; Chu, C. Impact behaviors of poly-lactic acid based biocomposite reinforced with unidirectional high-strength magnesium alloy wires. *Prog. Nat. Sci. Mater. Int.* **2014**, 24, 472–478. [CrossRef]

- 18. Wilson, C.J.; Clegg, R.E.; Leavesley, D.I.; Pearcy, M.J. Mediation of Biomaterial–Cell Interactions by Adsorbed Proteins: A Review. *Tissue Eng.* **2005**, *11*, 1–18. [CrossRef]
- 19. Falde, E.J.; Yohe, S.T.; Colson, Y.L.; Grinstaff, M.W. Superhydrophobic materials for biomedical applications. *Biomaterials* **2016**, *104*, 87–103. [CrossRef]
- 20. Li, Y.; Liu, G.; Zhai, Z.; Liu, L.; Li, H.; Yang, K.; Tan, L.; Wan, P.; Liu, X.; Ouyang, Z.; et al. Antibacterial properties of magnesium in vitro and in an in vivo model of implant-associated methicillin-resistant Staphylococcus aureus infection. *Antimicrob. Agents Chemother.* **2014**, *58*, 7586–7591. [CrossRef]
- 21. Robinson, D.A.; Griffith, R.W.; Shechtman, D.; Evans, R.B.; Conzemius, M.G. In vitro antibacterial properties of magnesium metal against Escherichia coli, Pseudomonas aeruginosa and Staphylococcus aureus. *Acta Biomater.* **2010**, *6*, 1869–1877. [CrossRef] [PubMed]
- 22. Rahim, M.I.; Eifler, R.; Rais, B.; Mueller, P.P. Alkalization is responsible for antibacterial effects of corroding magnesium. *J. Biomed. Mater. Res. Part A* **2015**, *103*, 3526–3532. [CrossRef] [PubMed]
- 23. Qin, H.; Zhao, Y.; Cheng, M.; Wang, Q.; Wang, Q.; Wang, J.; Jiang, Y.; An, Z.; Zhang, X. Anti-biofilm properties of magnesium metal via alkaline pH. *RSC Adv.* **2015**, *5*, 21434–21444. [CrossRef]
- 24. Rodríguez-Sánchez, J.; Pacha-Olivenza, M.Á.; González-Martín, M.L. Bactericidal effect of magnesium ions over planktonic and sessile Staphylococcus epidermidis and Escherichia coli. *Mater. Chem. Phys.* **2019**, 221, 342–348. [CrossRef]
- 25. Hickey, D.J.; Muthusamy, D.; Webster, T.J. Electrophoretic deposition of MgO nanoparticles imparts antibacterial properties to poly-L-lactic acid for orthopedic applications. *J. Biomed. Mater. Res. Part A* **2017**, 105, 3136–3147. [CrossRef]
- 26. Ma, R.; Lai, Y.X.; Li, L.; Tan, H.L.; Wang, J.L.; Li, Y.; Tang, T.T.; Qin, L. Bacterial inhibition potential of 3D rapid-prototyped magnesium-based porous composite scaffolds—An in vitro efficacy study. *Sci. Rep.* **2015**, 5, 13775. [CrossRef]
- Fernández-Calderón, M.C.; Cifuentes, S.C.; Pacha-Olivenza, M.A.; Gallardo-Moreno, A.M.; Saldaña, L.; González-Carrasco, J.L.; Blanco, M.T.; Vilaboa, N.; González-Martín, M.L.; Pérez-Giraldo, C. Antibacterial effect of novel biodegradable and bioresorbable PLDA/Mg composites. *Biomed. Mater.* 2017, 12, 015025.
   [CrossRef]
- 28. Ferrández-Montero, A.; Lieblich, M.; González-Carrasco, J.L.; Benavente, R.; Lorenzo, V.; Detsch, R.; Boccaccini, A.R.; Ferrari, B. Development of biocompatible and fully bioabsorbable PLA/Mg films for tissue regeneration applications. *Acta Biomater.* **2019**. [CrossRef]
- 29. Harris, L.G.; Richards, R.G. Staphylococci and implant surfaces: A review. *Injury* 2006, 37, S3–S14. [CrossRef]
- 30. Pacha-Olivenza, M.A.; Gallardo-Moreno, A.M.; Méndez-Vilas, A.; Bruque, J.M.; González-Carrasco, J.L.; González-Martín, M.L. Effect of UV irradiation on the surface Gibbs energy of Ti6Al4V and thermally oxidized Ti6Al4V. *J. Colloid Interface Sci.* **2008**, 320, 117–124. [CrossRef]
- 31. Van Oss, C.J.; Chaudhury, M.K.; Good, R.J. Monopolar surfaces. *Adv. Colloid Interface Sci.* **1987**, 28, 35–64. [CrossRef]
- 32. Van Oss, C.J.; Good, R.J.; Chaudhury, M.K. Additive and nonadditive surface tension components and the interpretation of contact angles. *Langmuir* **1988**, *4*, 884–891. [CrossRef]
- 33. Van Oss, C.J.; Ju, L.; Chaudhury, M.K.; Good, R.J. Estimation of the polar parameters of the surface tension of liquids by contact angle measurements on gels. *J. Colloid Interface Sci.* **1989**, *128*, 313–319. [CrossRef]
- 34. Gomes, I.B.; Simões, M.; Simões, L.C. The effects of sodium hypochlorite against selected drinking water-isolated bacteria in planktonic and sessile states. *Sci. Total Environ.* **2016**, *565*, 40–48. [CrossRef] [PubMed]
- 35. Gallardo-Moreno, A.M.; Vadillo-Rodríguez, V.; Perera-Núñez, J.; Bruque, J.M.; González-Martín, M.L. The zeta potential of extended dielectrics and conductors in terms of streaming potential and streaming current measurements. *Phys. Chem. Chem. Phys.* **2012**, *14*, 9758–9767. [CrossRef] [PubMed]
- 36. Yang, J.; Bei, J.; Wang, S. Enhanced cell affinity of poly (D,L-lactide) by combining plasma treatment with collagen anchorage. *Biomaterials* **2002**, *23*, 2607–2614. [CrossRef]

Coatings 2019, 9, 814 13 of 13

37. Cai, K.; Yao, K.; Cui, Y.; Yang, Z.; Li, X.; Xie, H.; Qing, T.; Gao, L. Influence of different surface modification treatments on poly(D,L-lactic acid) with silk fibroin and their effects on the culture of osteoblast in vitro. *Biomaterials* **2002**, *23*, 1603–1611. [CrossRef]

- 38. Onder, O.C.; Nazeer, M.A.; Yilgör, E.; Yilgör, I. Spontaneous formation of microporous poly(lactic acid) coatings. *Prog. Org. Coat.* **2018**, 125, 249–256. [CrossRef]
- 39. Li, J.; Li, Z.; Ye, L.; Zhao, X.; Coates, P.; Caton-Rose, F. Structure and biocompatibility improvement mechanism of highly oriented poly(lactic acid) produced by solid die drawing. *Eur. Polym. J.* **2017**, *97*, 68–76. [CrossRef]
- 40. Li, Z.; Zhao, X.; Ye, L.; Coates, P.; Caton-Rose, F.; Martyn, M. Fibrillation of chain branched poly (lactic acid) with improved blood compatibility and bionic structure. *Chem. Eng. J.* **2015**, 279, 767–776. [CrossRef]
- 41. Paragkumar, N.T.; Edith, D.; Six, J.L. Surface characteristics of PLA and PLGA films. *Appl. Surf. Sci.* **2006**, 253, 2758–2764. [CrossRef]
- 42. Van Oss, C.J. Interfacial Forces in Aqueous Media, 2nd ed.; CRC Press: Boca Raton, FL, USA, 2006.
- 43. Kolská, Z.; Kasálková, N.S.; Siegel, J.; Švorčík, V. Electrokinetic Potential for Characterization of Nanosctructured Solid Flat Surfaces. *J. Nano Res.* **2013**, 25, 31–39. [CrossRef]
- 44. Bastekova, K.; Guselnikova, O.; Postnikov, P.; Elashnikov, R.; Kunes, M.; Kolska, Z.; Švorčík, V.; Lyutakov, O. Spatially selective modification of PLLA surface: From hydrophobic to hydrophilic or to repellent. *Appl. Surf. Sci.* **2017**, 397, 226–234. [CrossRef]
- 45. Zhang, R.; Ma, P.X. Porous poly(L-lactic acid)/apatite composites created by biomimetic process. *J. Biomed. Mater. Res.* **1999**, 45, 285–293. [CrossRef]
- 46. Kokubo, T.; Kushitani, H.; Sakka, S.; Kitsugi, T.; Yamamuro, T. Solutions able to reproduce in vivo surface-structure changes in bioactive glass-ceramic A-W3. *J. Biomed. Mater. Res.* **1990**, 24, 721–734. [CrossRef]
- 47. Meng, Z.X.; Li, H.F.; Sun, Z.Z.; Zheng, W.; Zheng, Y.F. Fabrication of mineralized electrospun PLGA and PLGA/gelatin nanofibers and their potential in bone tissue engineering. *Mater. Sci. Eng. C* **2013**, *33*, 699–706. [CrossRef]
- 48. Babaie, E.; Ren, Y.; Bhaduri, S.B. Microwave sintering of fine grained MgP and Mg substitutes with amorphous tricalcium phosphate: Structural, and mechanical characterization. *J. Mater. Res.* **2016**, *31*, 995–1003. [CrossRef]
- 49. Babaie, E.; Lin, B.; Goel, V.K.; Bhaduri, S.B. Evaluation of amorphous magnesium phosphate (AMP) based non-exothermic orthopedic cements. *Biomed. Mater.* **2016**, *11*, 055010. [CrossRef]
- 50. Combes, C.; Rey, C. Amorphous calcium phosphates: Synthesis, properties and uses in biomaterials. *Acta Biomater.* **2010**, *6*, 3362–3378. [CrossRef]
- 51. Tamimi, F.; Le Nihouannen, D.; Bassett, D.C.; Ibasco, S.; Gbureck, U.; Knowles, J.; Wright, A.; Flynn, A.; Komarova, S.V.; Barralet, J.E. Biocompatibility of magnesium phosphate minerals and their stability under physiological conditions. *Acta Biomater.* **2011**, *7*, 2678–2685. [CrossRef]
- 52. Katsikogianni, M.; Missirlis, Y.F.; Harris, L.; Douglas, J. Concise review of mechanisms of bacterial adhesion to biomaterials and of techniques used in estimating bacteria-material interactions. *Eur. Cells Mater.* **2004**, *8*, 37–57. [CrossRef] [PubMed]
- 53. Gallardo-Moreno, A.M.; Navarro-Pérez, M.L.; Vadillo-Rodríguez, V.; Bruque, J.M.; González-Martín, M.L. Insights into bacterial contact angles: Difficulties in defining hydrophobicity and surface Gibbs energy. *Colloids Surf. B Biointerfaces* **2011**, *88*, 373–380. [CrossRef] [PubMed]



© 2019 by the authors. Licensee MDPI, Basel, Switzerland. This article is an open access article distributed under the terms and conditions of the Creative Commons Attribution (CC BY) license (http://creativecommons.org/licenses/by/4.0/).